Batteries & Supercaps

Research Article
doi.org/10.1002/batt.202200544

Chemistry Europe
European Chemical Societies Publishing

www.batteries-supercaps.org

Balancing Partial Ionic and Electronic Transport for Optimized Cathode Utilization of High-Voltage $LiMn_2O_4/Li_3InCl_6$ Solid-State Batteries

Theodoor A. Hendriks,[a] Martin A. Lange,[b] Ellen M. Kiens,[c] Christoph Baeumer,[c] and Wolfgang G. Zeier*[a, b]

Their suggested stability towards high-voltage cathode materials makes halide-based solid electrolytes currently an interesting class of ionic conductors for solid-state batteries. Especially the $LiMn_2O_4$ spinel cathode active material is of interest due to its slightly higher nominal voltage and more resilience to overcharging compared to $LiCoO_2$ and $LiNi_xMn_yCo_2O_2$ cathodes. Typically, a standard ratio of active material to solid electrolyte is used in composites for solid-state batteries. However, for ideal transport properties, and thus to achieve balanced and optimal partial-conductivities, this ratio needs to be re-optimized each time the material basis is changed. In this work, we show transport in the composite measured through both DC polarization as well as transmission line modeling of the impedance spectra. By balancing the partial transport parameters of the composite, an optimum capacity of the solid-state batteries is achieved. This work shows characterization and optimization of transport is required for unlocking the full potential of solid-state batteries.

Introduction

Increased demands for electronics portability and mobility have made lithium-ion batteries the system of choice for energy storage. Currently, a transition from liquid electrolytes to solid electrolytes is explored due to concerns about the flammability of organic solvents,[1,2] all of which may be overcome in the solid-state.[1,3] Inorganic solid electrolytes with high ionic conductivities above $1\,mS\,cm^{-1}$ are considered good replacements.[4–6] A promising class of solid electrolytes with these high conductivities is based on thiophosphates such as the argyrodite-type materials Li_6PS_5X (X = Cl, Br, I),[7] or Li_3PS_4[8,9] and $Li_{10}GeP_2S_{12}$.[10] In addition to their high ionic conductivities, these materials exhibit advantageous mechanical properties such as malleability, which leads to their prominent use in solid-state batteries.[3,11–15]

However, commonly used solid electrolyte materials, when used as a catholyte in a cathode composite, are outside their narrow thermodynamic stability window,[1,13,16] and decomposition reactions occur. Despite their instability, lithium argyrodites have been used as catholytes in composites in combination with $LiNi_xMn_yCo_zO_2$-based cathode active materials,[11,17–19] and active materials with specific protective coatings.[13,20–23] However, as coatings only seem to delay decomposition but cannot entirely prevent it,[21,24] more stable solid electrolytes are still being sought.

In the search for more stable materials, lithium metal halides are an interesting class of solid electrolytes that, through recent advances in synthesis methods,[25] can achieve lithium-ion conductivities in the range of $1\,mS\,cm^{-1}$.[25] While this conductivity is not sufficient for high electrode loadings,[26] it is an indication of their potential for use in solid-state batteries.

These lithium metal halides seem to exhibit an intrinsic stability at higher potentials and therefore may be ideally suited for high-voltage cathodes. Li_3InCl_6, for instance, has shown a high voltage stability up to 4.3 V vs. Li/Li^+,[27] and even has the possibility to be synthesized in a H_2O-mediated approach.[28] Because of this, the use of $LiMn_2O_4$ as active material seems interesting due to a similar capacity of $148\,mAh\,g^{-1}$ theoretically and $120\,mAh\,g^{-1}$ practically, as well as the slightly higher nominal voltage compared to $LiCoO_2$ or $LiNi_xMn_yCo_zO_2$, and its higher resiliency to overcharging.[29,30] Furthermore, $LiMn_2O_4$ can be used as a stepping stone to even higher voltage materials such as $LiNi_{0.5}Mn_{1.5}O_4$.[30,31] The latter has recently been shown to work in combination with argyrodite,[32] or with the halide Li_3YCl_6,[33] when sufficient coating is used.

When preparing solid-state batteries, composite cathodes are needed. For these composites of cathode active material and catholyte, a standard weight ratio of 70/30 is often used. This is historically based on the paper by Kitaura et al.[34]

[a] Dr. T. A. Hendriks, Prof. W. G. Zeier
Helmholtz Institut Münster (IEK-12)
Forschungszentrum Jülich
Corrensstrasse 46, D-48149 Münster (Germany)
E-mail: wzeier@uni-muenster.de
[b] Dr. M. A. Lange, Prof. W. G. Zeier
Institute of Inorganic and Analytical Chemistry
University of Münster
Corrensstrasse 30, D-48149 Münster (Germany)
[c] E. M. Kiens, Prof. C. Baeumer
MESA + Institute for Nanotechnology
University of Twente
P. O. Box 217, Enschede 7500 AE (The Netherlands)

Supporting information for this article is available on the WWW under https://doi.org/10.1002/batt.202200544

Research Article
doi.org/10.1002/batt.202200544
Chemistry Europe
European Chemical Societies Publishing

optimizing the ratio of Li_3PS_4 to Li_xCoO_2 and later by Zhang et al.[11] for $Li_{10}GeP_2S_{12}$ and Li_xCoO_2. An optimum ratio is necessary, because a perfect percolation in the composite cathode is required to ensure that sufficient ions and electrons are always available. In other words, the composite microstructure, and with it both the ionic and electronic partial conductivities, needs to be optimized to mediate the high tortuosity.[35,36] Whenever the material choices for the cathode composite changes, the optimum ratios of the compositions needs to be found for optimal transport characteristics, because the partial resistances within the composite do not scale linearly with the volume fractions of the constituents.[37] For instance, too much cathode active material prevents sufficient ionic transport pathways and too much catholyte prevents sufficient electronic pathways.[11] These partial conductivities of the composite are not only a function of the volume ratios of its constituents, but also of their particle sizes.[17,32] Consequently, re-optimization is necessary whenever other materials, other particle sizes, or the distribution of particle sizes changes.

Inspired by the promising possibility of using a halide-based solid electrolyte as catholyte together with a spinel cathode, in this work we explore solid-state batteries based on Li_3InCl_6 and $LiMn_2O_4$. To achieve this, the volume ratio in composite cathodes is varied and analyzed by measuring the partial ionic and electronic conductivities, as obtained from DC polarization as well as transmission line modeling of the impedance spectra. By analyzing the transport parameters, this work shows that optimum cycling conditions are found whenever the ratio of the partial ionic and electronic conductivities lies around unity. Using X-ray photoemission spectroscopy in combination with transport analyses, we show that chemical decomposition occurs despite the electrochemical stability of the catholyte. Overall, this work emphasizes that, in order to achieve optimum cell performance in solid-state batteries, the ratio of the components needs to be analyzed and optimized based on the underlying partial transport characteristics.

Results and Discussion

Halide-based solid electrolytes as catholytes

A large fraction of solid-state battery research employs Li_6PS_5Cl or derivatives as the solid electrolyte in solid-state batteries, either as the separator or the catholyte in the composite cathode. In principle, stable cycling has been reported for $LiNi_xMn_yCo_zO_2$ cathode active materials.[17–19] For long-term stable cycling, protection concepts are being developed as degrading interfaces are found when the oxide-based active materials are in contact with these sulfides, as chemical and electrochemical decomposition is favored.[22,38] Nevertheless, while sulfide-based solid-state batteries with $LiNi_xMn_yCo_zO_2$ are promising, high-voltage spinels cannot be used as the high potentials lead to too much degradation.[39] Further, halide-based solid electrolytes cannot be used at the anode as fast reduction of the metal halide occurs.[40] Therefore, in recent literature, Li_6PS_5Cl is used as an additional protection layer for the lithium metal halide separator.[19,20,40] This bilayer setup helps with protection of the halide solid electrolyte from the anode and protection of the sulfide solid electrolyte from the high cathode potentials. Nevertheless, recent work suggests some underlying chemical instability.[19,20,41] Therefore, in this work, the Li_3InCl_6 halide solid electrolyte is also inserted as protection layer between the Li_6PS_5Cl and cathode composite.

Figure 1 shows a direct comparison of different catholytes when using the high-voltage spinel. With Li_6PS_5Cl as the catholyte, only low capacities are found and cell cycling barely occurs due to known decomposition of the sulfide with the spinel.[18] In contrast, using Li_3InCl_6 as a catholyte and protection layer, better cell cycling can be observed. Clearly, for high-voltage cathode active materials, halide-based solid electrolytes are needed. However, as solid-state batteries need an ideal percolation in the composite cathode,[42] the typically observed optimum ratios in the composite may not necessarily be the same when the materials basis is changed. Therefore, in-depth transport measurements and cycling are needed to establish these optimum ratios.

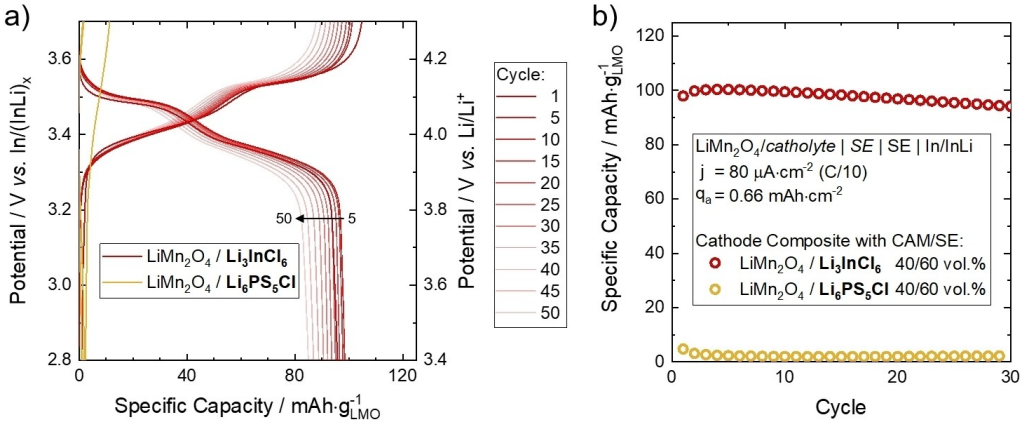

Figure 1. a) Charge discharge potential as a function of specific capacity and b) specific capacity as a function of cycles, to visualize the stark difference between the halide catholyte and when Li_6PS_5Cl is used as catholyte in contact with $LiMn_2O_4$ cathode active materials.

Partial ionic and electronic transport

Recent work has shown that especially the effective ionic and electronic transport of composites,[35,36] and with it the microstructure[32,43] and tortuosity,[44,45] need to be considered. For instance, Bielefeld et al.[43] show that for sufficient rates, at least an ionic conductivity of 10 $mS\,cm^{-1}$ is needed for solid-state battery cycling at 1 C. Work by Ohno et al.[45] shows that without fast effective transport in Li–S-solid-state batteries, high overpotentials are found and that in principle any addition of a non-ionically conducting species will deteriorate the effective ionic conductivity fast. Recent work further corroborates that inhomogeneous reaction fronts can be found in solid-state batteries if the ionic and electronic partial conductivity are not balanced.[36] Clearly, for an electrochemical reaction to occur and for fast kinetics, both electrons and ions need to be supplied in a fast and balanced manner.

In general, there are two approaches to measure the partial ionic and electronic conductivities of cathode composites. First, DC polarization can be used as shown by Ohno et al.[37,45] and Dewald et al.[35] by using symmetric cell configurations with electronic and ionic blocking electrodes, respectively. Second, transmission line modeling of the impedance spectra can be employed in symmetric cells,[17,45] or even in solid-state battery cell configurations.[44,46] While DC measurements obtain reliable transport parameters within the cathode composites, transmission line modeling can provide a more in-depth information on the occurring interfacial processes in solid-state batteries.

Here, in order to ascertain the use of transmission line modeling in half-cell configuration, both polarization experiments and transmission line modeling of the half-cells are performed. The DC polarization is obtained on the composites by subjecting the symmetric cells to DC voltage perturbations (5, −10, 20, 30 mV) in order to obtain their resistivity and determine the partial conductivities for each volume fraction. A representative measurement is shown in Figure 2(a–f), all measurements can be found in the Supporting Information (Figures S2–S7a–f).

In order to determine the standard deviation in the partial conductivities, data are measured in triplicates. Transmission line modeling is performed on the impedance spectra of discharged composites in the half-cells, to confirm the transport properties with respect to the pristine cathode composites. Here, the partial transport parameters of the cathode composite should hold regardless of the symmetric cell configuration during DC measurement or when going to the half-cell configuration: 'In/InLi | Li_6PS_5Cl | Li_3InCl_6 | *cathode composite*' upon impedance measurements in-between cycling. As the open circuit voltage of a pristine half-cell is around 3 V vs. Li/Li^+, the cathode active material $Li_xMn_2O_4$ is around $x \approx 1$ and assumed to be the same during the DC measurements. Therefore, in order to verify the partial transport of half-cells, they need to be measured at an equal state (i.e., discharged). To allow for thermodynamic equilibrium, impedance spectroscopy is performed after an hour of constant potential after discharge. Example impedance spectra can be found in Figure 2(g and h). Using Kramers-Kronig analyses, the reliable frequency range for the impedance analyses is identified (see Figure S8). A non-Faradaic transmission line model is used that accounts for the different processes in the cell, as shown schematically in Figure 2(i and j). The non-Faradaic approach was chosen, as the lithiated $LiMn_2O_4$ should exhibit minimal charge transfer resistance. For an in-depth discussion on the possible transmission line model configurations, we refer to previous literature on porous film electrodes and solid-state battery composites.[17,44–49] In short, in order to ensure a reliable fitting, a purely electronic resistor was used here for the partial electronic transport. For the ionic transport, a combined resistor and constant-phase element in parallel was needed. This is in contrast to the usual behavior of sulfide catholytes, where often only a resistor element can be found in the respective transmission line model.[17] At this stage we assume this is related to the slower ionic transport in Li_3InCl_6. When modeling the transmission line, measurements were also performed in triplicates to obtain a standard deviation of the extracted transport parameters.

Figure 3(a) shows the conductivities of $LiMn_2O_4/Li_3InCl_6$ cathode composites at different volume fractions. Both DC polarization determined partial conductivities are shown together with the obtained values from transmission line modeling. At first glance, DC polarization gives a much cleaner trend of the transport data. Nevertheless, conductivities determined by both approaches shows values within their standard deviations for all volume fractions. This shows that both the DC polarization method as well as transmission line modeling can be used to determine partial transport properties of cathode composites, and in the end optimize the transport.

In theory, an optimal cathode performance should be achieved when neither ionic nor electronic conductivity is the rate-limiting factor.[36] In other words, while for a high-rate solid-state battery one needs fast transport in general, balanced transport is needed to effectively address most active material in a composite. Therefore, the volume ratio of the active material and catholyte needs to be optimized. Whereas previous work used trial-and-error approaches to find the optimum,[11] measuring the partial transport presents a more systematic and reliable approach.[17,35] Here, based on the obtained transport data, the optimum ratio of cathode active material and the halide-based catholyte is at a volume ratio of 40/60, respectively. A direct comparison to literature with the data by Minnmann et al.[17] on a composite of $LiNi_{0.8}Co_{0.1}Mn_{0.1}O_2/Li_6PS_5Cl$ shows that our composite with spinel active material and halide as catholyte needs slightly less solid electrolyte to achieve the best transport balancing (see Figure 3b).

However, in the case of the spinel and halide-based solid electrolyte, the ionic and electronic conductivity is between one and two orders of magnitude lower than when using the fast ion-conducting sulfide solid electrolyte Li_6PS_5Cl as catholyte. For high-rate cells, much faster transport needs to be achieved, needing electronic additives and faster ionic conductors.

Research Article
doi.org/10.1002/batt.202200544
Chemistry Europe
European Chemical Societies Publishing

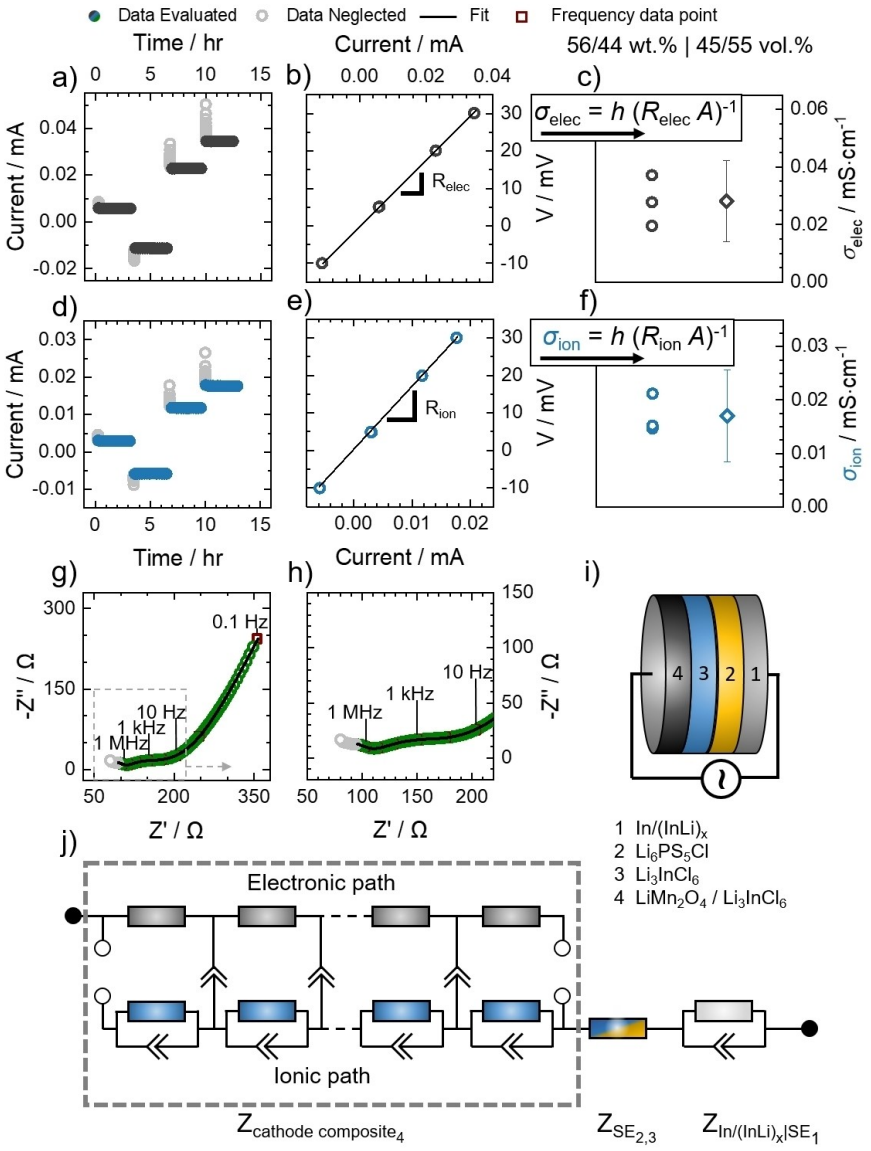

Figure 2. a) Representative DC measurement of electronic current over time. b) Electronic resistance line showing Ohmic behavior. c) Calculated partial electronic conductivity based on triplicate data collection. The diamond represents the average and the given measurement uncertainty represents two times the standard deviation. d) Representative DC measurement of ionic current over time. e) Ionic resistance line showing Ohmic behavior. f) Calculated partial ionic conductivity. The diamond represents the average and the given measurement uncertainty represents two times the standard deviation. g) Representative impedance spectrum with neglected data due to too high Kramers-Kronig error in grey, and the transmission line model (j) fit in black line. h) Zoom-in of (g). i) Model of the cell geometry upon impedance measurements. j) Transmission line model used to model the impedance data during cycling after a voltage hold of 1 hour after discharge voltage cutoff.

Electrochemical cycling

Cycling of solid-state battery half-cells allows to determine accessible capacities and the fading behavior. Figure 4(c) shows the charge-discharge behavior of the first cycle of all cathode composites and Figure 4(d) the capacities as a function of cycle number (for Coulomb efficiencies we refer to Figure S15). Consecutive cycling shows that optimizing transport is beneficial for cycling longevity. Increased fading of the capacities can be found for increased content of cathode active material, Furthermore, fast fading is observed for the volume fractions of solid electrolyte below 0.6 as shown in Figure 4(e).

In order to understand the fading behavior, X-ray photoelectron spectroscopy is used (see Supporting Information) to obtain elemental compositions and valence states in the cycled composites of three best performing compositions. The spectra (Figures S16–S18) show strong indications for decomposition with the potential decomposition products In_2O_3 and MnO after cycling, which were absent in the uncycled cells. This indicates that a strong interfacial reaction has taken place. A discussion of the spectra can be found in the Supporting Information. Very recently it was suggested that the halides might already decompose while operated within their electrochemical stability window, as there might be chemical instability.[33] Our

Research Article
doi.org/10.1002/batt.202200544
Chemistry Europe
European Chemical Societies Publishing

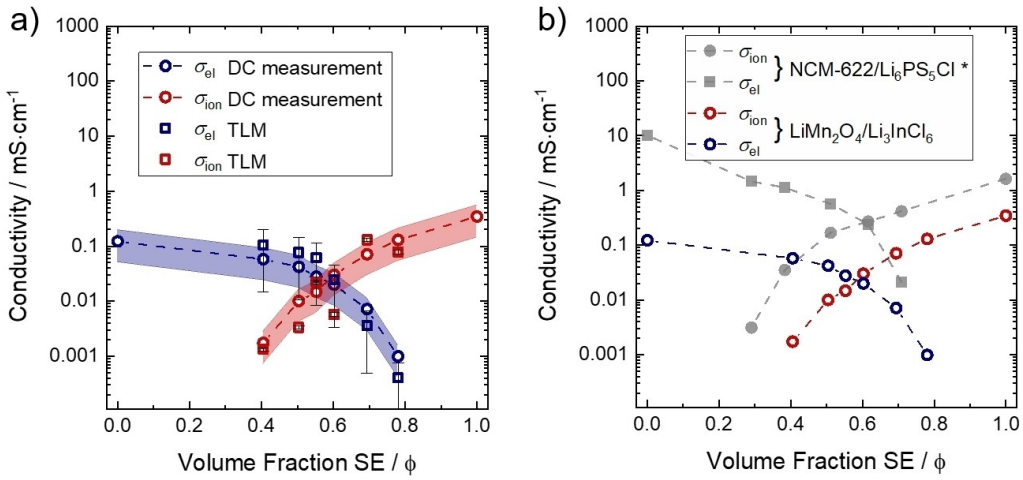

Figure 3. a) Conductivity over volume fraction of solid electrolyte showing in shaded areas the error in the conductivity as measured by DC measurements, and given measurement uncertainty represents the variation in the conductivity as obtained from transmission line modeling. b) Conductivity over volume fraction of solid electrolyte showing the differences between the work on NCM-622/Li_6PS_5Cl cathode composites from Ref. [17] and this work on $LiMn_2O_4$/Li_3InCl_6 cathode composites.

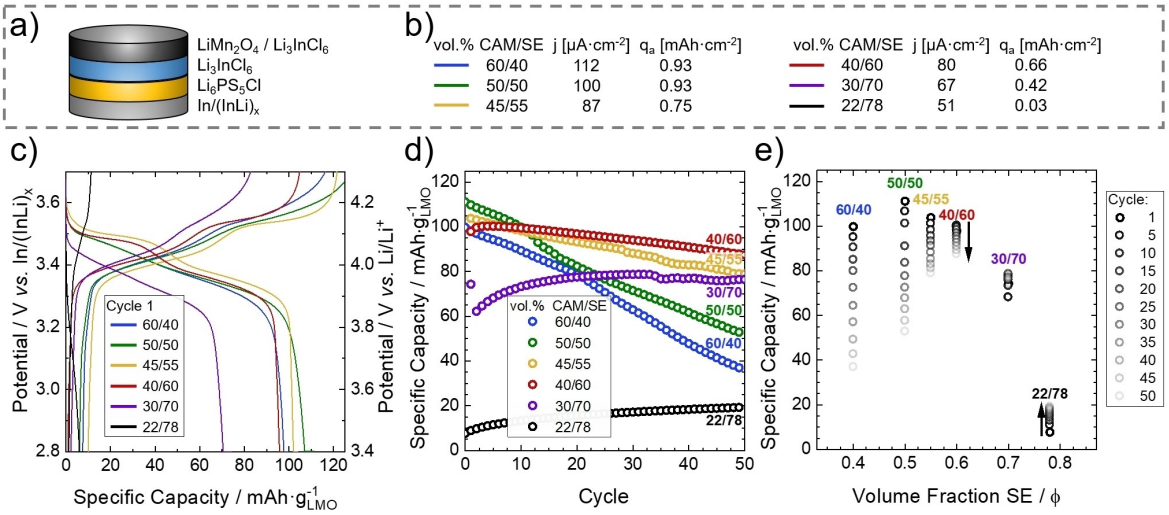

Figure 4. a) Schematic cell setup and b) the applied current densities and obtained areal capacities of the first cycle depending on the volume% cathode active material to solid electrolyte. c) The potential as function of the specific capacity for the first cycle of different ratios of cathode active material to solid electrolyte. Volume ratios of cathode active material to solid electrolyte of 30/70 and especially 22/78 show lower specific discharge capacity for their first cycle. d) Cycling behavior of the different ratios inside the cathode composite. When the volume fraction of cathode active material in the composite is very high, large fading can be observed. When it is low, only marginal specific capacity can be obtained. e) Fading behavior in steps of five cycles for the different ratios in the cathode composite.

findings align with this observation. At this stage, it seems reasonable to assume that higher content of active materials leads to more interfacial contact area and, hence, more severe fading behavior due to chemical decomposition at the interface.

Discussion on optimum transport parameters

As shown above, measuring the partial ionic and electronic conductivities can guide the optimization of cathode composites. Three major conclusions can be drawn:

1) A balanced transport is needed to achieve high capacities in solid-state batteries, as schematically shown in Figure 5(b). For optimal use of all cathode active materials, both ions and electrons need to be supplied at the same rate, i.e., the ratio of $\sigma_{ion}/\sigma_{elec}$ needs to be close to unity. Figure 5(a) shows that when this ratio is close to unity (in this case $\sigma_{ion}/\sigma_{elec} = 0.23 \pm 0.12$), the maximum capacity can be achieved in this study for a composite of $LiMn_2O_4$ and Li_3InCl_6. To further corroborate this, comparing our data to that of a system using Li_6PS_5Cl and $LiNi_{0.8}Co_{0.1}Mn_{0.1}O_2$, given in Ref. [17] (Figure S13b), shows again that to unlock an

Research Article
doi.org/10.1002/batt.202200544
Chemistry Europe
European Chemical Societies Publishing

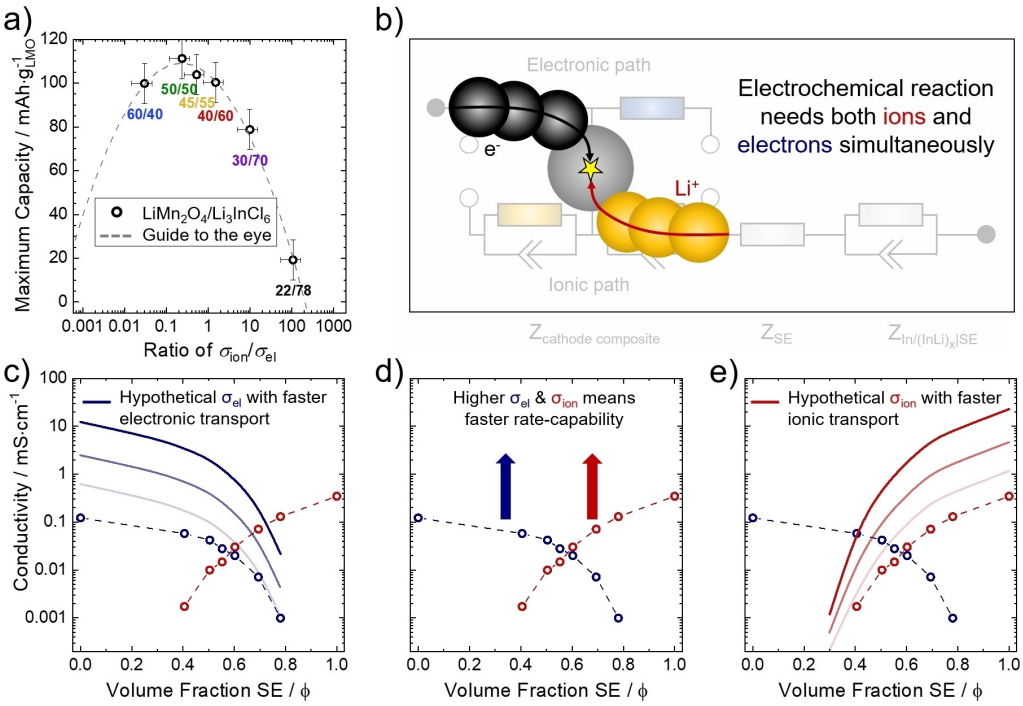

Figure 5. a) Maximum specific capacity of the first cycle for different ratios of the $LiMn_2O_4$ cathode active material to the Li_3InCl_6 catholyte. Vertical uncertainties represent standard deviation in capacity, horizontal uncertainties represent two standard deviations in the ratio of conductivities. Dashed grey line provides a guide to the eye. b) Schematic representation of the transport of both Li^+-ions and electrons through the cathode composite. Both are needed simultaneously for an electrochemical reaction. Therefore, optimal performance can be expected around $\sigma_{ion}/\sigma_{el} \approx 1$. Schematic improvements of transport by adding an electronically conductive additive in c) or faster ionic transport in e). Combined (d), they allow for composites capable of higher rates. For simplicity no strong change in tortuosity is assumed.

optimal capacity of the first cycle and achieve balanced transport, a $\sigma_{ion}/\sigma_{elec}$ ratio close to unity is ideal.

Nevertheless, we expect this to be dependent on the current density. At lower rates, even unbalanced transport can lead to a full cathode active material utilization (Figure S13b, C/10 data) as the cycling will be slow enough. Therefore, unbalanced transport is only acceptable as long as the partial transport is just "fast enough" for the applied rate.

2) Comparing the data using Li_3InCl_6 and $LiMn_2O_4$ to the work by Minnmann et al.,[17] using the faster conductors Li_6PS_5Cl as catholyte and $LiNi_{0.8}Co_{0.1}Mn_{0.1}O_2$ as cathode active material, shows that in the first case the partial ionic and electronic conductivities are an order of magnitude lower (Figure 3b). This suggests that good performance at higher C-rate will not be possible as advocated by Bielefeld et al.[43] However, further optimizations are possible and we show this schematically in Figure 5(c–e). For instance, if one were to optimize on the electronic conductivity *via* conductive additives, the optimum ratio would shift to higher solid electrolyte content. Hence, faster solid electrolytes would be needed to retain a high fraction of cathode active material. This suggests that any time a different solid electrolyte is used as catholyte, a different additive, or a different cathode active material is used, the transport in the composites needs to be optimized.

3) Even in the most optimally balanced case, fading will still occur if too much active material is employed (see Figure 4e), as higher active material content will mean more surface area for decomposition.[50] Hence, transport optimization is not the only parameter that needs to be optimized, protective coatings of active materials remain important.

Conclusion

Optimal cell cycling in solid-state batteries with a composite cathode consisting of $LiMn_2O_4$ spinel active material and Li_3InCl_6 halide catholyte can be achieved when the transport within the composite is optimized to be balanced. By measuring partial ionic and electronic transport in these composite cathodes via DC polarization and impedance spectroscopy (analyzed via a transmission line model), we show that unlocking the full potential of the active material can be achieved when the ratio of both ionic and electronic conductivities is around unity. Nevertheless, balanced transport does not protect from decomposition and the used combination of $LiMn_2O_4$ and Li_3InCl_6 would, if used in the future, still need protection concepts on the active material, especially at high cathode active material ratios in the composite. Overall, this work shows the importance of optimizing solid-state battery performances, and shows that a detailed look on the underlying transport in the composite cathodes is required.

Research Article
doi.org/10.1002/batt.202200544

Acknowledgements

C. B. has received funding from the European Research Council (ERC) under the European Union's Horizon 2020 research and innovation program under grant agreement No. 101040669. Open Access funding enabled and organized by Projekt DEAL.

Conflict of Interest

The authors declare no conflict of interest.

Data Availability Statement

The data that support the findings of this study are available from the corresponding author upon reasonable request.

Keywords: electrochemical impedance spectroscopy · halide solid electrolyte · solid electrolyte · solid state batteries · transmission line model

[1] J. Janek, W. G. Zeier, *Nat. Energy* **2016**, *1*, 16141.
[2] A. Manthiram, X. Yu, S. Wang, *Nat. Rev. Mater.* **2017**, *2*, 16103.
[3] S. Randau, D. A. Weber, O. Kötz, R. Koerver, P. Braun, A. Weber, E. Ivers-Tiffée, T. Adermann, J. Kulisch, W. G. Zeier, F. H. Richter, J. Janek, *Nat. Energy* **2020**, *5*, 259–270.
[4] Y. Kato, S. Hori, T. Saito, K. Suzuki, M. Hirayama, A. Mitsui, M. Yonemura, H. Iba, R. Kanno, *Nat. Energy* **2016**, *1*, 16030.
[5] S. Ohno, A. Banik, G. F. Dewald, M. A. Kraft, T. Krauskopf, N. Minafra, P. Till, M. Weiss, W. G. Zeier, *Prog. Energy* **2020**, *2*, 022001.
[6] Y. S. Jung, D. Y. Oh, Y. J. Nam, K. H. Park, *Isr. J. Chem.* **2015**, *55*, 472–485.
[7] A. Gautam, M. Sadowski, M. Ghidiu, N. Minafra, A. Senyshyn, K. Albe, W. G. Zeier, *Adv. Energy Mater.* **2021**, *11*, 2003369.
[8] K. Homma, M. Yonemura, T. Kobayashi, M. Nagao, M. Hirayama, R. Kanno, *Solid State Ionics* **2011**, *182*, 53–58.
[9] Z. Liu, W. Fu, E. A. Payzant, X. Yu, Z. Wu, N. J. Dudney, J. Kiggans, K. Hong, A. J. Rondinone, C. Liang, *J. Am. Chem. Soc.* **2013**, *135*, 975–978.
[10] S. P. Culver, A. G. Squires, N. Minafra, C. W. F. Armstrong, T. Krauskopf, F. Böcher, C. Li, B. J. Morgan, W. G. Zeier, *J. Am. Chem. Soc.* **2020**, *142*, 21210–21219.
[11] W. Zhang, D. A. Weber, H. Weigand, T. Arlt, I. Manke, D. Schröder, R. Koerver, T. Leichtweiss, P. Hartmann, W. G. Zeier, J. Janek, *ACS Appl. Mater. Interfaces* **2017**, *9*, 17835–17845.
[12] J. Ruhl, L. M. Riegger, M. Ghidiu, W. G. Zeier, *Adv. Energy Sustain. Res.* **2021**, *2*, 2000077.
[13] R. Koerver, I. Aygün, T. Leichtweiß, C. Dietrich, W. Zhang, J. O. Binder, P. Hartmann, W. G. Zeier, J. Janek, *Chem. Mater.* **2017**, *29*, 5574–5582.
[14] A. Sakuda, A. Hayashi, M. Tatsumisago, *Sci. Rep.* **2013**, *3*, 2261.
[15] L. L. Baranowski, C. M. Heveran, V. L. Ferguson, C. R. Stoldt, *ACS Appl. Mater. Interfaces* **2016**, *8*, 29573–29579.
[16] F. Walther, R. Koerver, T. Fuchs, S. Ohno, J. Sann, M. Rohnke, W. G. Zeier, J. Janek, *Chem. Mater.* **2019**, *31*, 3745–3755.
[17] P. Minnmann, L. Quillman, S. Burkhardt, F. H. Richter, J. Janek, *J. Electrochem. Soc.* **2021**, *168*, 040537.
[18] J. Auvergniot, A. Cassel, J.-B. Ledeuil, V. Viallet, V. Seznec, R. Dedryvère, *Chem. Mater.* **2017**, *29*, 3883–3890.
[19] T. Koç, F. Marchini, G. Rousse, R. Dugas, J.-M. Tarascon, *ACS Appl. Energ. Mater.* **2021**, *4*, 13575–13585.
[20] C. Wang, J. Liang, J. Luo, J. Liu, X. Li, F. Zhao, R. Li, H. Huang, S. Zhao, L. Zhang, J. Wang, X. Sun, *Sci. Adv.* **2021**, *7*, DOI 10.1126/sciadv.abh1896.
[21] F. Walther, F. Strauss, X. Wu, B. Mogwitz, J. Hertle, J. Sann, M. Rohnke, T. Brezesinski, J. Janek, *Chem. Mater.* **2021**, *33*, 2110–2125.
[22] S. P. Culver, R. Koerver, W. G. Zeier, J. Janek, *Adv. Energy Mater.* **2019**, *9*, 1900626.
[23] R. S. Negi, P. Minnmann, R. Pan, S. Ahmed, M. J. Herzog, K. Volz, R. Takata, F. Schmidt, J. Janek, M. T. Elm, *Chem. Mater.* **2021**, *33*, 6713–6723.
[24] G. Oh, M. Hirayama, O. Kwon, K. Suzuki, R. Kanno, *Chem. Mater.* **2016**, *28*, 2634–2640.
[25] T. Asano, A. Sakai, S. Ouchi, M. Sakaida, A. Miyazaki, S. Hasegawa, *Adv. Mater.* **2018**, *30*, 1803075.
[26] A. Bielefeld, D. A. Weber, R. Rueß, V. Glavas, J. Janek, *J. Electrochem. Soc.* **2022**, *169*, 020539.
[27] S. Wang, Q. Bai, A. M. Nolan, Y. Liu, S. Gong, Q. Sun, Y. Mo, *Angew. Chem. Int. Ed.* **2019**, *58*, 8039–8043; *Angew. Chem.* **2019**, *131*, 8123–8127.
[28] X. Li, J. Liang, N. Chen, J. Luo, K. R. Adair, C. Wang, M. N. Banis, T. Sham, L. Zhang, S. Zhao, S. Lu, H. Huang, R. Li, X. Sun, *Angew. Chem. Int. Ed.* **2019**, *58*, 16427–16432; *Angew. Chem.* **2019**, *131*, 16579–16584.
[29] M. M. Thackeray, *Prog. Solid State Chem.* **1997**, *25*, 1–71.
[30] M.-J. Lee, S. Lee, P. Oh, Y. Kim, J. Cho, *Nano Lett.* **2014**, *14*, 993–999.
[31] G. Q. Liu, L. Wen, Y. M. Liu, *J. Solid State Electrochem.* **2010**, *14*, 2191–2202.
[32] H. J. Lee, X. Liu, Y. Chart, P. Tang, J.-G. Bae, S. Narayanan, J. H. Lee, R. J. Potter, Y. Sun, M. Pasta, *Nano Lett.* **2022**, *22*, 7477–7483.
[33] J. Jang, Y.-T. Chen, G. Deysher, D. Cheng, S.-Y. Ham, A. Cronk, P. Ridley, H. Yang, B. Sayahpour, B. Han, W. Li, W. Yao, E. A. Wu, J.-M. Doux, L. H. B. Nguyen, J. A. S. Oh, D. H. S. Tan, Y. S. Meng, *ACS Energy Lett.* **2022**, *7*, 2531–2539.
[34] H. Kitaura, A. Hayashi, T. Ohtomo, S. Hama, M. Tatsumisago, *J. Mater. Chem.* **2011**, *21*, 118–124.
[35] G. F. Dewald, S. Ohno, J. G. C. Hering, J. Janek, W. G. Zeier, *Batteries & Supercaps* **2021**, *4*, 183–194.
[36] R. Bradbury, G. F. Dewald, T. Arlt, J. Janek, W. G. Zeier, S. Ohno, *ChemRxiv.* **2021**, DOI https://doi.org/10.33774/chemrxiv-2021-vwnpt-v2.
[37] S. Ohno, W. G. Zeier, *Accounts Mater. Res.* **2021**, *2*, 869–880.
[38] L. Zhou, N. Minafra, W. G. Zeier, L. F. Nazar, *Acc. Chem. Res.* **2021**, *54*, 2717–2728.
[39] K. Kim, D. Park, H.-G. Jung, K. Y. Chung, J. H. Shim, B. C. Wood, S. Yu, *Chem. Mater.* **2021**, *33*, 3669–3677.
[40] L. M. Riegger, R. Schlem, J. Sann, W. G. Zeier, J. Janek, *Angew. Chem. Int. Ed.* **2021**, *60*, 6718–6723; *Angew. Chem.* **2021**, *133*, 6792–6797.
[41] C. Rosenbach, F. Walther, P. Hartmann, T. A. Hendriks, S. Ohno, J. Janek, W. G. Zeier, *Adv. Energy Mater.* **2022**, DOI 10.1002/aenm.202203673.
[42] T. Shi, Q. Tu, Y. Tian, Y. Xiao, L. J. Miara, O. Kononova, G. Ceder, *Adv. Energy Mater.* **2020**, *10*, 1902881.
[43] A. Bielefeld, D. A. Weber, J. Janek, *ACS Appl. Mater. Interfaces* **2020**, *12*, 12821–12833.
[44] N. Kaiser, S. Spannenberger, M. Schmitt, M. Cronau, Y. Kato, B. Roling, *J. Power Sources* **2018**, *396*, 175–181.
[45] S. Ohno, C. Rosenbach, G. F. Dewald, J. Janek, W. G. Zeier, *Adv. Funct. Mater.* **2021**, *31*, 2010620.
[46] V. Miß, A. Ramanayagam, B. Roling, *ACS Appl. Mater. Interfaces* **2022**, *14*, 38246–38254.
[47] J. Bisquert, *Phys. Chem. Chem. Phys.* **2000**, *2*, 4185–4192.
[48] Z. Siroma, N. Fujiwara, S. Yamazaki, M. Asahi, T. Nagai, T. Ioroi, *Electrochim. Acta* **2015**, *160*, 313–322.
[49] Z. Siroma, T. Sato, T. Takeuchi, R. Nagai, A. Ota, T. Ioroi, *J. Power Sources* **2016**, *316*, 215–223.
[50] W. Zhang, T. Leichtweiß, S. P. Culver, R. Koerver, D. Das, D. A. Weber, W. G. Zeier, J. Janek, *ACS Appl. Mater. Interfaces* **2017**, *9*, 35888–35896.

Manuscript received: December 13, 2022
Revised manuscript received: January 25, 2023
Accepted manuscript online: January 26, 2023
Version of record online: February 8, 2023